Thermal analysis of a nanofluid free jet impingement on a rotating disk using volume of fluid in combination with discrete modelling

Mostafa Mahdavi[a], Mohsen Sharifpur[a,b], Josua P. Meyer[a] and Lingen Chen[c,*]

[a]Department of Mechanical and Aeronautical Engineering, University of Pretoria, Private Bag X20, Hatfield, 0028, Pretoria, South Africa
[b]Institute of Research and Development, Duy Tan University, Da Nang 550000, Vietnam
[c]Institute of Thermal Science and Power Engineering, Wuhan Institute of Technology, Wuhan, 430205, China

*Corresponding author. Institute of Thermal Science and Power Engineering, Wuhan Institute of Technology, Wuhan, 430205, China. Email: lingenchen@hotmail.com

Highlights

- Nanofluid free jet impingement on hot stationary and rotating disk is numerically studied.
- Volume of Fluid method is used combining with Discrete Phase Model to track nanoparticles.
- Six stages are found during jet impingement until steady-state condition is reached.
- No splatter of droplets is observed in the rotating disk.
- Five flow regions are identified on rotating disk regarding thermal and velocity boundary layers.

Abstract

The objective of this research is to analyse the heat transfer characteristics of air/nanofluid jet cooling flow on a hot circular rotating disk and track the possible fate of nanoparticles. Computational methods are employed to initially solve the air and liquid multiphase flow in ANSYS Fluent 19.3 by considering the importance of surface tension between two phases through the volume of fluid model. Subsequently, the nanoparticles are injected through the nozzle into the jet liquid to calculate nanoparticles distribution via pre-defined user functions. The impacts of parameters such as nanoparticles volume fraction and disk rotation are evaluated. The patterns of the jet flow from inlet until steady-state condition shows that there exist six stages of fluid flow for a stationary hot disk, while splattering of droplets disappears when the disk starts rotating. In spite of the positive impact of nanoparticles for rotating disk, larger torque is required for higher nanofluid volume fraction to enhance heat transfer due to increase in viscosity. Also, the trend for heat transfer coefficient identifies five flow regions from the stagnation point to the edge of the rotating disk.

Keywords: Nanofluid jet impingement; ANSYS Fluent; Volume of fluid; Discrete phase model; Hot rotating disk

Nomenclature

A_p	particle projected area [m^2]
C_c	Cunningham correction factor
C_D	drag coefficient
C_{ML}	rotational coefficient
c_p	specific heat [J/kg.K]
D	disk diameter [m]
d_p	particle diameter [m]
d_c	water molecule diameter [m]
D_T	thermophoresis diffusion coefficient [m^2/s]
G_b	generation of turbulence kinetic energy due to buoyancy [N/m^2s]
G_k	generation of turbulence kinetic energy due to the mean velocity gradients [N/m^2s]
H	nozzle to disk distance [m]
h	heat transfer coefficient [$W/m^2.K$]
k	Thermal conductivity [W/m.K]
K_B	Boltzmann constant [$m^2.kg/K.s^2$]
m_p	particle mass [kg]
Nu	Nusselt number
Pr	Prandtl number
q	laminar and turbulent heat flux [W/m^2]
Re	jet Reynolds number
Re_p	particle Reynolds number
Re_{ω_p}	particle angular Reynolds number
Re_r	disk rotational Reynolds number
S_k, S_ε	user-defined source terms [N/m^2s]
t_v	nano-layer thickness [nm]
Δt_p	particle time step [s]
T_{fr}	reference temperature [k]
V,u	velocity [m/s]
Y_M	contribution of the fluctuating dilatation in compressible turbulence to the overall dissipation rate [N/m^2s]

Greek letters

α	phase volume fraction
ϕ	particle volume fraction
$\dot{\gamma}$	shear rate [1/s]
κ	turbulent kinetic energy [m^2/s^2]
μ	viscosity [Pa.s]
μ_t	turbulent viscosity [Pa.s]
ω_p	particle angular velocity [1/s]
ω_r	disk angular velocity [1/s]
Ω_l	relative particle-liquid angular velocity [1/s]
ρ	density [kg/m^3]
σ	surface tension [N/m]
σ_k, σ_ε	turbulent constant
ζ_i	Gaussian white noise random number

Subscript

ip	impingement point
j	jet
W, l	water
nf	nanofluid
p	particle

1. Introduction

One of the most common effective ways of cooling hot surfaces in many industries is to spray or imping cooler fluid. Due to thin thermal and viscous boundary layers on the hot surface, rapid heat and mass transfers are achieved in some essential industries such as textile and wood, metal sheet manufacturing, turbine blades, combustion engine, etc.

Considering the extensive applications of jet cooling systems in engineering sections, a large number of experimental and numerical studies have been conducted throughout years, from simple cases to higher complexity. For the purpose of reviewing literature in this section, it is essential to take the following remarks into account: The difference between free and confined jet cooling systems, geometry of the hot surfaces from circular and rectangular to curvy shapes, non-boiling or boiling flows on the surfaces, stationary or dynamic objects like rotating disks, using air or liquid for cooling, applying nanoparticles in the flow to improve the heat transfer [[1], [2], [3], [4], [5], [6], [7]].

Most of the experimental studies for jet cooling have been concerned with air or liquid, and especially water, in Ref. [[8], [9], [10], [11], [12], [13], [14], [15], [16], [17], [18], [19], [20], [21], [22], [23], [24], [25]]. At the early stage, researchers mainly focused on conventional and most applicable geometries like rectangular and circular shapes with air and water as the cooling medium, with taking the rotating impact of the hot surface into account [[8], [9], [10], [11], [12],[26], [27], [28], [29], [30]]. Carper et al. [8] conducted an experiment on a hot rotating disk via oil jet with different Prandtl number from 87 to 400. They found out the heat transfer was not affected by the nozzle to hot disk distance as long as the flow exiting the nozzle remained laminar. However, they reported the possible change of -slope in Nu number on the disk could result from the developing flow on the hot surface from laminar to transition. The other parameters investigated in their experiment consisted of disk rotational Reynolds number, jet flow Reynolds number, disk to nozzle diameter ratio, jet Prandtl number and the effects of asymmetric impingement. They developed a correlation for average Nu number on the cooling in terms of disk rotational Reynolds number, jet flow Reynolds number and Prandtl number.

On the other hand, some other authors have studied jet flows for rotating disks in turbulent conditions for both air and water [[8], [9], [10], [11],15]. Gabour and Lienhard [11] investigated the role of surface roughness on heat transfer for liquid jet Reynolds number above 20, 000. They stated that the wall could be assumed smooth in terms of stagnation Nusselt number under some specific values of non-dimensional roughness height. They showed that the nozzle to target spacing could not influence the Nusselt number. Although, Goldstein et al. [9] reported that the spacing in air impingement jet could be important in changing the recovery factor, which is a function of wall and jet temperature and velocity. They also mentioned that the thickness of thermal boundary layer on the hot surface might highly depend on nozzle inside diameter and Reynolds number. Depending on the conditions of the flow and hot surface geometry, the findings of researchers also have shown some discrepancies. For instance, Pachpute and Premachandran [20] stated that the nozzle to target spacing could play an important role on average Nusselt number, which was in opposition of findings by Baonga et al. [13]. Minagawa and Obi [12] used local velocity ratio as a contributing factor in rotating disk jet flows, while Jing-zhou [15] simply explained the changes in Nusselt number on a rotating disk via distance from the center of the disk to the radius. Baonga et al. [13] identified three significant regions in the jet flow on a hot disk: the impingement, parallel flow and the hydraulic jump regions.

One of the main attempts of researchers in jet cooling systems has been to enhance the efficiency of the heat transfer by manipulating of fluid characteristics and properties. In recent years, adding nanoparticles to the base fluid is becoming a popular method [[31], [32], [33]]. Nanoparticles are usually smaller than 100 nm and have minimum negative impacts on hydraulic features of the fluid flow. While with appropriate improvement of thermal conductivity, the heat transfer can be considerably enhanced due to higher conductivity of the

nanoparticles [[34], [35], [36], [37], [38]]. Considering this new technology, it has been a number of experimental studies of jet impingement nanofluid, either free or submerged jets, in recent years [[39], [40], [41], [42], [43], [44], [45], [46], [47], [48]]. One of the early experiments was conducted by Nguyen et al. [40] for submerged alumina nanofluid up to 6% vol. on a horizontal hot disk with uniform flux in turbulent regime. They found that the increase in particles volume fraction may improve the heat transfer up to a certain amount. Higher fraction up to 6% vol. might deteriorate the rate of heat transfer, especially with the possibility of sedimentation. They also reported that reducing nozzle to target spacing can have positive effects only up to a certain amount. On the contrary, the findings by Sorour et al. [46] showed that higher nanoparticle volume fraction up to even 8.5% increased the heat transfer and the ratio of spacing and nozzle diameter had a minimum impact on thermal features of nanofluid flow. Modak et al. [47] reported that the nanoparticles presence could improve Nusselt number up to 90% compared to the pure water jet. Keeping the flow in turbulent regime in all cases, no noticeable enhancement was observed in heat transfer by changing the spacing between nozzle and hot plate. They also indicated that maximum Nusselt number always occurred at the stagnation point (impingement), and decreased towards the downstream away from the impingement point. They developed a Nusselt number correlation in terms of Reynolds number, Prandtl number and the ratio of spacing to nozzle diameter, with the accuracy of ±30%. More accurate Nusselt number correlation for nanofluid jet flow was proposed by Barewar et al. [41] with ±15% in terms of nanoparticles volume fraction, Peclet number, Reynold number, Prandtl number and ratio of spacing to nozzle diameter.

Due to many limitations in any experiment in terms of some measurements, numerical methods can be useful tools to reveal all aspects of the tests. The complexity of nanofluid jet impingement can be concerned with flow regime, heat transfer, interaction between two phases of air and liquid, dispersed nanoparticles in the flow, volume fraction distribution and possible sedimentation. Some of these conditions have been investigated by authors in recent years [[49], [50], [51], [52], [53], [54], [55], [56]]. As expected, some authors focused on deep understanding of free or submerged jet flows without nanoparticles, and especially with rotating disk, because of simpler nature of modelling. Laminar confined liquid jet impingement without nanoparticles was studied by Lallave et al. [49] on a hot rotating disk. They stated that the rotation of the disk could only dominate the heat transfer when the multiplication of Reynold and Ekman numbers is below 0.075. They employed Ekman number to non-dimensionally define the effects of rotating disk, instead of rotational Reynolds number used by Oguic et al. [54]. Oguic et al. [54] modelled a hot rotating disk via direct numerical simulations (DNS) and in a turbulent jet flow without nanoparticles. Lamraoui et al. [50] assumed nanofluid as Newtonian as well as non-Newtonian and used a single-phase approach with complete uniform distribution of nanofluid during the confined jet laminar flow, meaning uniform properties. Yang et al. [52] simulated a free water jet on a hot plate and employed Standard k-ε and volume of fluid (VOF) multiphase to model turbulence and surface tension between air and water. Free jet impingement of different nanofluids on a hot rectangular plate was numerically solved by Rehman et al. [53]. Continuous surface force (CSF) model as a part of the VOF model was used to track the surface between air and fluid. Also, Standard k-ε was employed to solve turbulence in the flow. The impacts of nanoparticles were included through replacing the fluid properties with mixture properties of nanofluid. Peng et al. [56] conducted a nanofluid simulation in a confined jet flow by mixture and Eulerian-Eulerian models. They considered nanoparticles as the second phase in the flow.

The work mentioned above shows that most of the researches for nanofluid cooling jet on a hot surface is experimental and there is a limited number of simulation for the nanofluid free jet. Also, modelling of nanoparticles in fluid flows is mainly concerned with only one liquid phase in the domain and simple geometries such as tubes or cavities [[57], [58], [59]]. Lack of enough modelling studies of nanoparticles inside a jet flow with considering the air and liquid interaction is the main motivation of this investigation. In this study, nanofluid jet impingement on a hot circular geometry will be simulated by including the surface tension between air and liquid. Nanoparticles will be injected in the flow and tracked by using the discrete phase model (DPM), and the obtained concentration distribution will be applied to the fluid properties through some user functions. Eventually, rotation as RPM will be added to the hot surface to investigate the effects of cooling jet on dynamic geometry.

2. Geometry and mathematical formulation

2.1. Problem statement

The initial geometry is based on an experimental study conducted by Zeitoun and Ali [39]. The minimum nozzle inside diameter is 3.9 mm, and the distance between nozzle and disk is kept 50 mm. The general arrangement of the nozzle, hot rotating disk and computational domain is shown in Fig. 1.

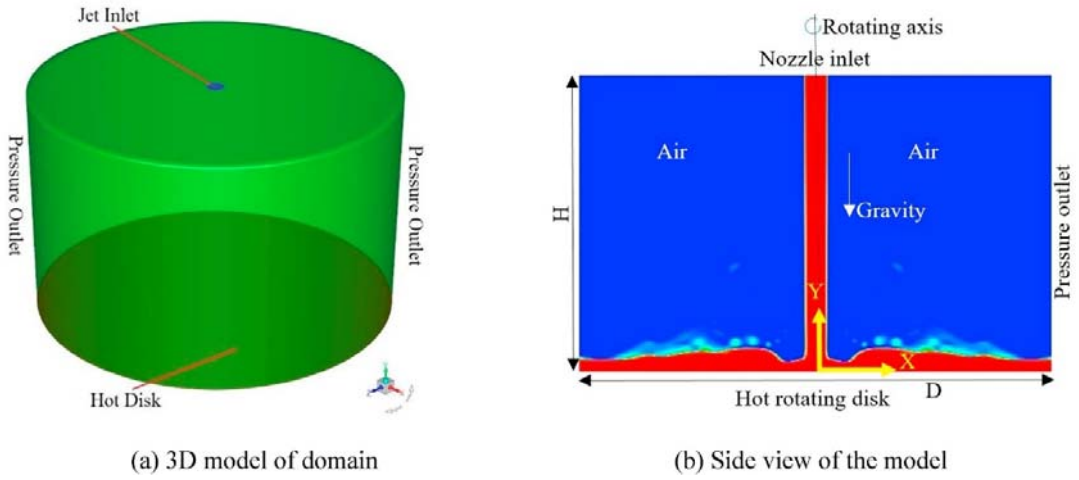

Fig. 1. General arrangement of the physical model for a jet flow impinging a rotating disk.

At the beginning of the simulation, the entire domain is filled with air. Then, flow is injected from the jet nozzle inlet into the domain until it hits the hot surface. Because of pressure boundary around the domain, liquid can exit without any backflow. The vertical centreline of the domain is in Y direction, and therefore the rotation can be added to the disk regarding this coordinate.

2.2. Mathematical equations: multiphase VOF model

Two phases are present in the computational domain, air as the primary and water/nanofluid as the secondary phase. Multiphase VOF model [60] assumes that the two-phase do not interfere in each other medium and the interface between them is mathematically calculated

in each computational cell by knowing the volume fraction of each phase and interaction surface tension force.

$$\begin{cases} \alpha = 1 & liquid \\ \alpha = 0 & air \\ 0 < \alpha < 1 & mixture \ \ \text{int}\, erface \end{cases} \tag{1}$$

Only one set of momentum and energy equations are solved. The flow is solved in unsteady frame and incompressible without exchange of any mass between phases. The interface between phases is obtained through solving the continuity equation for one of the phases:

$$\frac{\partial}{\partial t}\left(\alpha_i \rho_i\right) + \nabla . \left(\alpha_i \rho_i \overrightarrow{u}\right) = 0 \tag{2}$$

where α represents air/water volume fraction at the interface and *i* one of the phases.

Momentum and energy equations are as follows:

$$\frac{\partial\left(\rho \overrightarrow{u}\right)}{\partial t} + \nabla . \left(\rho \overrightarrow{u}\, \overrightarrow{u}\right) = -\nabla P + \nabla . \left(\mu \left(\nabla \overrightarrow{u}^{T} + \nabla \overrightarrow{u}\right)\right) + \rho \overrightarrow{g} + \sigma \chi \overrightarrow{\nabla} \alpha \tag{3}$$

$$\frac{\partial}{\partial t}\left(\rho E\right) + \nabla . \left(\rho E \overrightarrow{u}\right) = \nabla . \left(k \nabla T\right) \tag{4}$$

where *E*, *P* and *k* are energy, pressure and thermal conductivity, respectively. The last term in momentum equation is the surface tension force by CSF model [61], where σ and χ are surface tension and interface curvature obtained from continuum surface force model based on surface normal vector ñ, and defined as:

$$\chi = -\nabla . \tilde{n} \tag{5}$$

The energy term *E*, which represents $c_p T$, is obtained from the mass averaged specific heat and temperature of each phase as:

$$E = \frac{\sum_{i=1}^{i=2} \alpha_i \rho_i E_i}{\sum_{i=1}^{i=2} \alpha_i \rho_i} \tag{6}$$

Since the Reynolds number of the jet flow is above 4000, the flow needs to be solved via one of the turbulent models. A realizable *k-ε* model is numerically solved to estimate the fluctuating velocity and turbulent viscosity, being successfully used by other researchers [62,63]. The transport equations for the turbulent kinetic energy (κ), dissipation rate (ε) and viscosity are briefly presented as follows

$$\frac{\partial}{\partial x_i}\left(\rho \kappa u_i\right) = \frac{\partial}{\partial x_i}\left(\left[\mu + \frac{\mu_t}{\sigma_k}\right] \frac{\partial \kappa}{\partial x_i}\right) + G_k + G_b - \rho \varepsilon - Y_M + S_k \tag{7}$$

$$\frac{\partial}{\partial x_i}(\rho\varepsilon u_i) = \frac{\partial}{\partial x_i}\left(\left[\mu + \frac{\mu_t}{\sigma_\varepsilon}\right]\frac{\partial \varepsilon}{\partial x_i}\right) + \rho C_1 S\varepsilon - \rho C_2 \frac{\varepsilon^2}{\kappa + \sqrt{\nu\varepsilon}} + C_{1\varepsilon}\frac{\varepsilon}{\kappa}C_{3\varepsilon}G_b + S_\varepsilon \quad (8)$$

$$\mu_t = \rho C_\mu \frac{\kappa^2}{\varepsilon} \quad (9)$$

$$C_1 = \max\left[0.43, \frac{S\frac{\kappa}{\varepsilon}}{S\frac{k}{\varepsilon}+5}\right] \quad (10)$$

$$C_2 = 1.9, \sigma_k = 1.0, \sigma_\varepsilon = 1.2, C_{1\varepsilon} = 1.44 \quad (11)$$

$$C_\mu = \frac{1}{A_0 + A_s\frac{kU^*}{\varepsilon}}, \quad (12)$$

where $\sigma_k, C_2, \sigma_\varepsilon, A_0$ and $C_{1\varepsilon}$ are turbulent constant, and $\mu_t, G_k, G_b, Y_M, S_k$ and S_ε are turbulent viscosity, generation of turbulence kinetic energy due to the mean velocity gradients, generation of turbulence kinetic energy due to buoyancy, contribution of the fluctuating dilatation in compressible turbulence to the overall dissipation rate, and last two terms are user-defined source terms.

The required boundary conditions are consist of: no slip at the walls with zero velocity and turbulent variables, velocity inlet at the nozzle, uniform heat flux at the disk, zero volume fraction of air at the nozzle, and no entry of liquid flow from the outlet boundaries with volume fraction 1 for air backflow. The mathematical form of boundary conditions is as:

At the wall: $u = v = w = 0, q'' = constant, \omega \neq 0$ for the case of rotating disk.

At the nozzle inlet: $u = u_{inlet}, \alpha_{air} = 0$

At the outlet: $P = atmospheric, \alpha_{air-backflow} = 1$,

2.3. Fluid and nanofluid properties

Since there are 3 phases are present in the domain, the interactions between liquid (or nanofluid)-air and liquid-nanoparticles have to be treated individually. For the case of liquid-air, the properties are the volume average of the two phases on the interface cells, as [60]:

$$y = \alpha y_l + (1-\alpha)\, y_{air} \quad (13)$$

where *y* is the property of each phase.

The variation of temperature in the jet flow in this study can be from 25 °C up to 80 °C at the edge of the hot disk. Therefore, it is essential to use accurate correlations for water properties, as listed in Table 1 [64].

Table 1. Thermo-physical properties of water.

	$\rho\left(kg/m^3\right)$	$c_p\left(J/kg.K\right)$	$k\left(W/m.K\right)$	$\mu\left(kg/m.s\right)$
Water	$765.33+1.8142\times \mathrm{T}-0.0035\times \mathrm{T}^2$	$(28.07-0.2817\times \mathrm{T}+0.00125\times \mathrm{T}^2-2.48\mathrm{e}-6\times \mathrm{T}^3+1.857\mathrm{e}-9\times \mathrm{T}^4)\times 1000$	$-0.5752+0.006397\times \mathrm{T}-8.151\mathrm{e}-6\times \mathrm{T}^2$	$0.0967-8.207\mathrm{e}-4\times \mathrm{T}+2.344\mathrm{e}-6\times \mathrm{T}^2-2.244\mathrm{e}-9\times \mathrm{T}^3$

To calculate the nanofluid density, the following correlation is borrowed from Sharifpur et al. [65]:

$$\rho_{nf}=\frac{\sum_{k=1}^{2}\phi_k\rho_k}{(1-\phi)+8\phi(d_p/2+t_v)^3/d_p^3} \tag{14}$$

$$t_v=-0.0002833(d_p/2)^2+0.0475d_p/2-0.1417 \tag{15}$$

The other thermo-physical properties are given as follows [66]:

$$c_{P_{nf}}=\frac{\sum_{k=1}^{2}\phi\rho_k c_{P_k}}{\rho_{nf}} \tag{16}$$

$$\frac{k_{nf}}{k_w}=1+4.4\mathrm{Re}^{0.4}\,\mathrm{Pr}^{0.66}\left(\frac{T}{T_{fr}}\right)^{10}\left(\frac{k_p}{k_w}\right)\phi^{0.66} \tag{17}$$

$$\mathrm{Re}=\frac{\rho_w u_B d_p}{\mu_w} \tag{18}$$

$$u_B=\frac{2K_BT}{\pi\mu_w d_p^2} \tag{19}$$

$$\frac{\mu_{nf}}{\mu_w}=\frac{1}{1-34.87(d_p/d_c)^{-0.3}\phi^{1.03}} \tag{20}$$

The other important parameters in the interface of nanofluid and air are undoubtedly surface tension. The following correlation is used to present the surface tension at the interface [67,68]:

$$\frac{\sigma_{w-air}-\sigma_{nf-air}}{\sigma_{w-air}}=-7.773\times 10^{-3}\,\ln\left(\frac{\phi}{7.673\times 10^{-7}}+1\right) \tag{21}$$

2.4. Introducing nanoparticles in the fluid flow by discrete modelling

To obtain a correct distribution of nanoparticles in the flow, discrete phase model (DPM) is employed to track the particles in the Lagrangian frame until their final fate is revealed. Hence, a finite number of particles are tracked in each time step as a representative of other particles. The attempt is made to consider all the interaction forces involved. However, virtual mass and pressure gradient forces are found to be negligible and removed from calculations [69]. Newton's equation of force balance in the Lagrangian frame for nanoparticles is written in details as follows:

$$m_p \frac{du_p}{dt_p} = F_{drag} + m_p \frac{\vec{g}(\rho_p - \rho_l)}{\rho_p} + F_{lift} + F_{Magnus} + F_{thermo} + F_B \tag{22}$$

The effective forces on tracking nanoparticles in this equation are drag, gravity, lift, Magnus, thermophoretic and Brownian, and t_p is the particle travelling time in Lagrangian frame.

Drag force is [70]:

$$F_{drag} = \frac{m_p}{\tau} \frac{C_D Re_p}{24 C_c} (u_l - u_p) \tag{23}$$

$$\text{where } Re_p = \frac{\rho_l d_p |u_l - u_p|}{\mu_l} \tag{24}$$

Saffman lift force is [71]:

$$F_{lift} = 20.3 \mu_l d_p^2 (u_l - u_p) \sqrt{\frac{\dot{\gamma}\rho_l}{\mu_l}} \operatorname{sgn}(\dot{\gamma}) \tag{25}$$

where $\dot{\gamma}$ is the shear rate.

Magnus force is induced by rotation of the particle around its axis in the uniform flow [72]:

$$F_{Magnus} = \frac{1}{2} A_p C_{ML} \rho_c \frac{|u_l - u_p|}{|\Omega_l|} [(u_l - u_p) \times \Omega_l] \tag{26}$$

$$\text{where } \Omega_l = \frac{1}{2} \nabla \times u_l - \omega_p \tag{27}$$

$$C_{ML} = 0.45 + \left(\frac{Re_{\omega_p}}{Re_p} - 0.45 \right) exp\left(-0.05684 Re_{\omega_p}^{0.4} Re_p^{0.3} \right) \tag{28}$$

$$Re_{\omega_p} = \frac{\rho_l |\Omega_l| d_p^2}{4\mu_l} \tag{29}$$

Thermophoretic force is [73]:

$$F_{thermo} = -D_T \frac{\nabla T}{T} \tag{30}$$

$$\text{where } D_T = 0.78 \frac{\pi \mu_l^2 d_p}{\rho_l} \frac{k_l}{2k_l + k_p} \tag{31}$$

Brownian random force is [70]:

$$F_B = \zeta_i \sqrt{\frac{6\pi d_p \mu_l K_B T}{\Delta t_p}} \tag{32}$$

where ζ_i is the unit-variance random number produced by a Gaussian white noise process.

3. Grid study and model validation

Due to the complexity of the number of equations involved, it is necessary to study a wide variety of meshes to find the most suitable one for this unsteady case. The attempt is made to generate structure mesh all over the domain. Because of the unsteady nature of the flow and expensive running time of the simulations, only 30° segment of the model is created, and periodic boundary condition is applied on the sections, as shown in Fig. 2. It is noted that since the thin layer of fluid on the disk flows directly into the atmospheric condition, adding the size of the domain had no impacts on the results, and hence the geometry was chosen as Fig. 2.

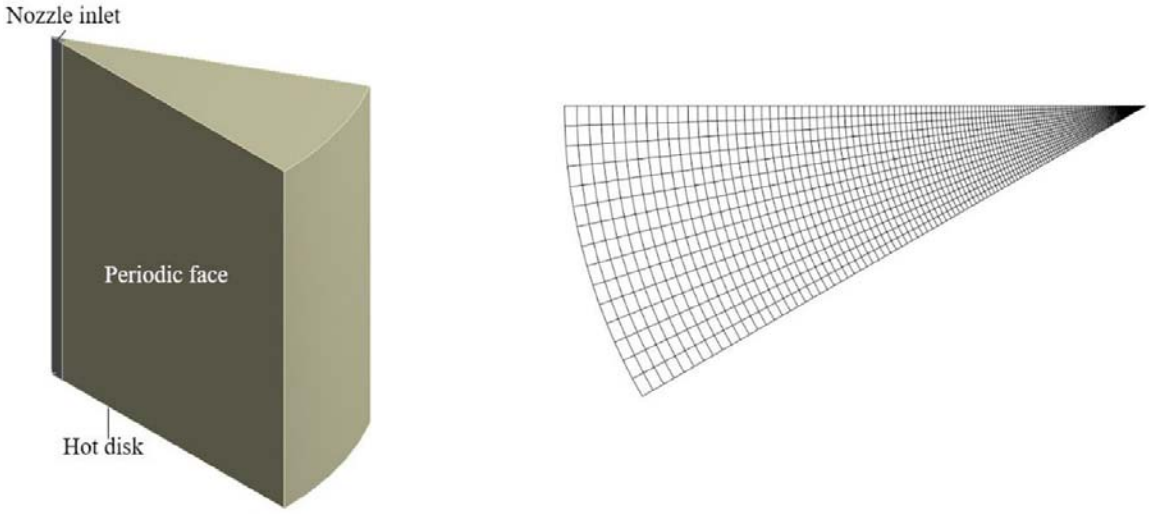

Fig. 2. Periodic geometry and generated mesh of the computational domain.

As explained, due to involvement of multiphase VOF model, turbulence, unsteady nature of the flow, impingement of liquid on a sold plate, solid disk rotation and using DPM, the simulation is highly sensitive to the mesh and convergence and correct solution only obtained for highly uniform and fine mesh close to the hot wall. The appropriate choice of the methods and models in CFD tools are as:

For fluid: VOF multiphase in implicit mode, Realizable k-ε turbulent model with Scalable wall function. For nanoparticles: using discrete model, including the particle forces as gravity, Brownian, drag, thermophoresis, lift and Magnus, input values for particles as nanoparticles diameter, velocity, temperature and mass law, including heat transfer law for nanoparticles.

For solver: using SIMPLE scheme, PRESTO! for pressure, Compressive for volume fraction and second-order upwind for other variables. The time step is chosen as 0.0001 s after try and error of many types of meshes.

The domain is based on the experimental work done by Zeitoun and Ali [39]. A Nusselt obtained from the test of water jet with 0.0039 m nozzle diameter and Reynolds number of 7190 is compared to those from each grid generated to achieve the best mesh for this study. The other input parameters such as jet velocity for simulations are calculated by the following correlations:

$$\mathrm{Re} = \frac{\rho\, u_{ip} D_{ip}}{\mu}, \quad D_{ip} = D_j \left(\frac{u_j}{u_{ip}}\right)^{0.5}, \quad u_{ip} = \sqrt{u_j^2 + 2gH} \tag{33}$$

where u_{ip} and D_{ip} are velocity and jet diameter at the impingement point, and are velocity and jet diameter at the nozzle. Regarding the obtained parameters and properties based on the average temperature of the jet and liquid film on the hot surface, Nusselt number is calculated by:

$$Nu = \frac{hD}{k}, \quad h = \frac{q}{(T_w - T_j)} \tag{34}$$

Table 2 lists the comparison between different meshes and Nusselt number obtained. The simulations are performed on a supercomputer cluster with 80 cores. Eventually, the best mesh generated is chosen 300 × 125 × 20 and total cells of 750, 000.

Table 2. Grid study – Mesh no. is longitudinal, radial and tangential.

Mesh size no.	Total no. of cells	Experiment Nu	Numerical Nu	No. of cells in boundary layer	Time step (s)	Running time (80 cores)	Error
150 × 40 × 18	108, 000	532	Divergence	1	0.001	1 day	–
300 × 85 × 25	637,500	532	270	2	0.0007	2 days	49%
300 × 40 × 8	96, 000	532	365	5	0.0005	1 day	32%
300 × 80 × 10	240, 000	532	440	5	0.0003	2 days	18%
300 × 80 × 10	240, 000	532	Divergence	5	0.0001	2 days	18%
300 × 125 × 20	750, 000	532	480	5	0.0003	3 days	10%
300 × 125 × 20	750, 000	532	498	8	0.0001	3 days	6%
380 × 165 × 32	2, 006, 400	532	498	13	0.0001	5 days	6%

At this stage, the validity of the methods and equations needs to be confirmed by comparing with literature. The Nu number obtained from the simulations for both water and alumina nanofluid of 1.7% vol is compared with experimental measurements by Zeitoun and Ali [39] in Fig. 3. The maximum error between the two results is below 11% in the worst case, and all below 10% for pure water. The accuracy of the numerical Nu number calculation drastically

decreases as the Reynolds number increases. It is noted that as the Reynolds number drops to around 4000, the possibility of percentage of transition flow at the hot surface may increase. This can be a contributing factor for higher error in lower Reynolds number in numerical modelling compared to experiment. In addition, lower Reynolds number leads to smaller and less changes in terms of heat transfer and Nusselt number, increasing the error in experimental measurements.

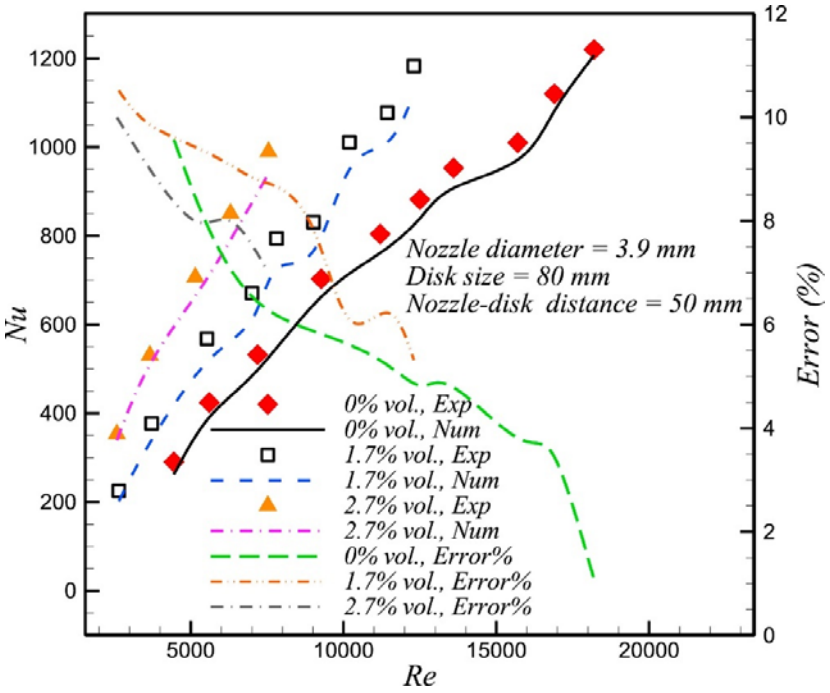

Fig. 3. Comparison of Nusselt number numerical calculations with experimental measurements for pure water and alumina nanofluid with 1.7% vol. conducted by Zeitoun and Ali [39].

3.1. Note - Guide study for free jet modelling

Due to the involvement of two different approaches of multiphase flows, and considering the transient nature of the flow, it is critical to find a method to avoid expensive simulations. Therefore, the following procedure is recommended for this kind of modelling to find the appropriate mesh and parameters required:

1. A 2D model is developed, and different meshes are generated to find the appropriate one with the capability of solving in the steady frame.
2. The results of steady-state solution are used to start the transient simulation with a gradual decrease in time step in each simulation. In this way, the optimum time step is obtained.
3. The thickness of the flow on the hot surface is monitored to ensure the number of computational cells inside the boundary layer is enough to capture the velocity and temperature profile.
4. The settings of modeling in the previous stage are used for the new 3D model. The results of steady-state similar to 2D model are also used here as initial values, and then the frame is changed to transient.

5. The results of the simulation are checked with experiment and confirmed. The accuracy of the models and mesh is confirmed, and other simulations can be solved in full transient manner.

4. Results and discussions

Due to the importance of cooling moving objects in industry, a rotating disk with uniform heat flux was studied here. A nanofluid cooling jet impinges on the hot surface and leaves the domain into the atmospheric air in ambient temperature.

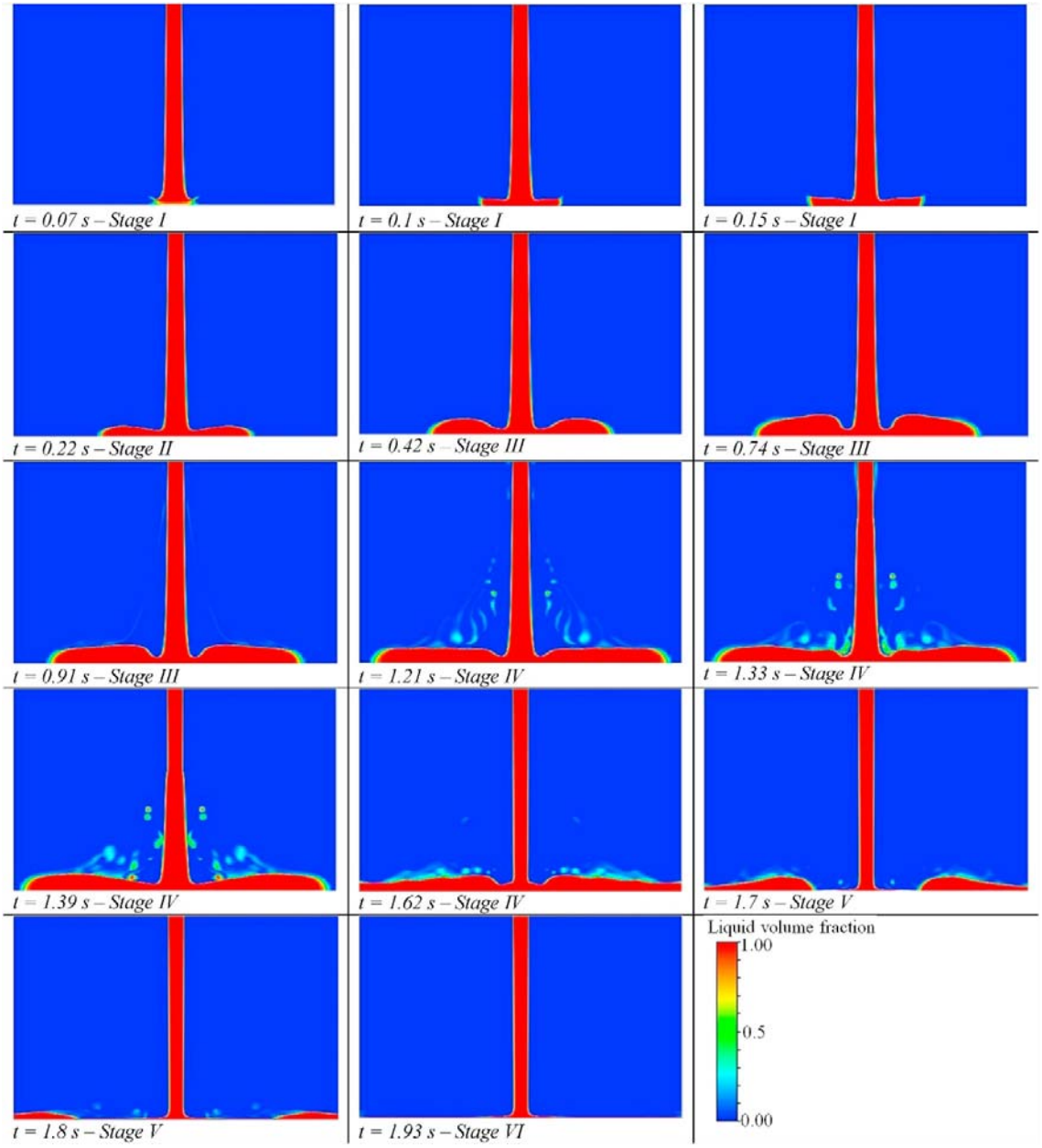

Fig. 4. Time evolution of jet impingement on a stationary hot disk from side view with Re = 7190.

The evolution of water jet impingement from nozzle inlet to the outlet of the domain is shown in Fig. 4. Before the jet reaches the disk, the diameter of the jet increases due to direct impact of surface tension (t = 0.07 s). After the impingement, a short parallel flow section is developed, and immediately after that, a hydraulic jump is initially formed at t = 0.22 s for Re = 7190. The hydraulic jump section is also reported by Baonga et al. [13] along with the parallel flow at the vicinity of the impingement region. The transition between forming of parallel flow to lamella [14,74] (or hydraulic jump section) continues until the full deposition [74] of the flow occurs towards the edge of the disk. The splatter of small water droplets starts at t = 1.21 s, and eventually returns to the deposition part at t = 1.62 s. These phenomena were also observed in the experiment conducted by Guo and Green [74]. Finally, the deposited flow will leave the domain to reach the steady fluid flow. Regarding the abovementioned details, a turbulent free liquid jet flow can be divided into the following stages until it reaches the steady-state condition:

(I) Impingement stage followed by the formation of initial parallel flow
(II) Formation of hydraulic jump (lamella)
(III) Deposition of liquid and extension towards the edge of the disk
(IV) The splatter of small droplets and return to the deposition
(V) Flattening of the deposition and leaving the disk
(VI) Steady-state flow

For comparing purposes, the evolution of water jet impingement for a rotating disk is also provided in Fig. 5. As can be seen, the droplets splatter stage does not occur on a rotating disk with RPM = 1000, because of strong acceleration in the radial direction. The deposition height and duration are also reduced as the flow on the disk does not have a chance to grow in vertical direction.

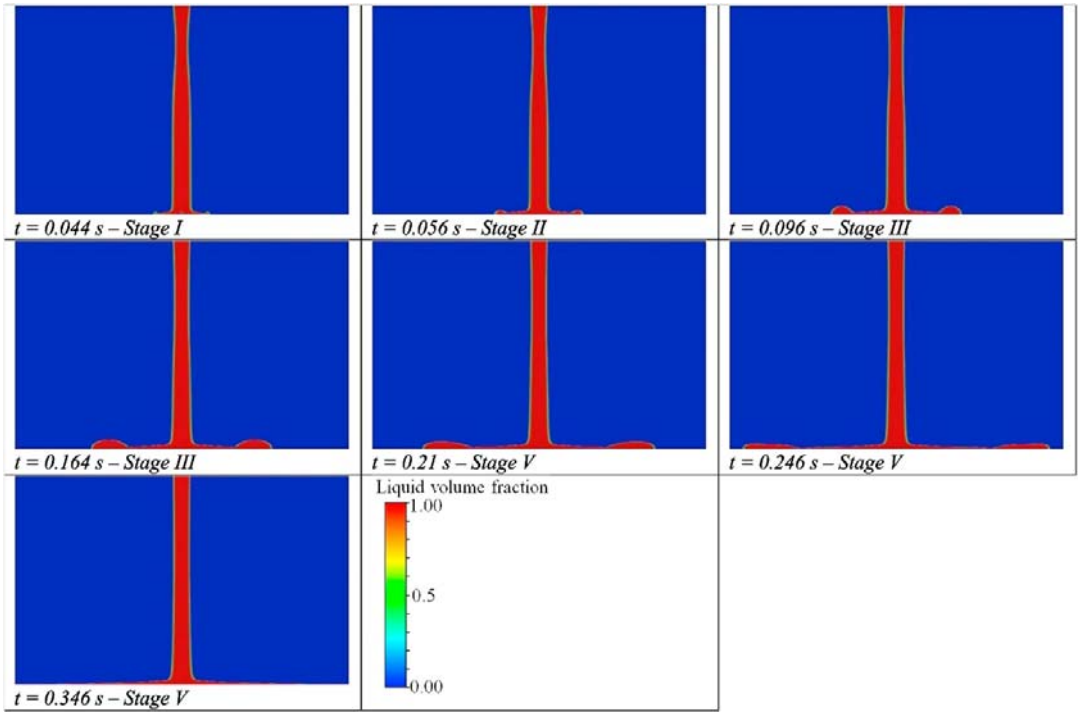

Fig. 5. Time evolution of jet impingement on a rotating hot disk from side view with Re = 7190 and RPM = 1000.

One of the other critical aspects of jet cooling can be the time required for dropping temperature to the desired value. The evolution of the surface temperature with time is presented in Fig. 6. It is observed that Re number is a contributing factor on the duration of cooling, the higher, the shorter of cooling. However, the jet velocity plays an important role as well, as lower velocity can make the process much slower, with slightly less dependency on Re number.

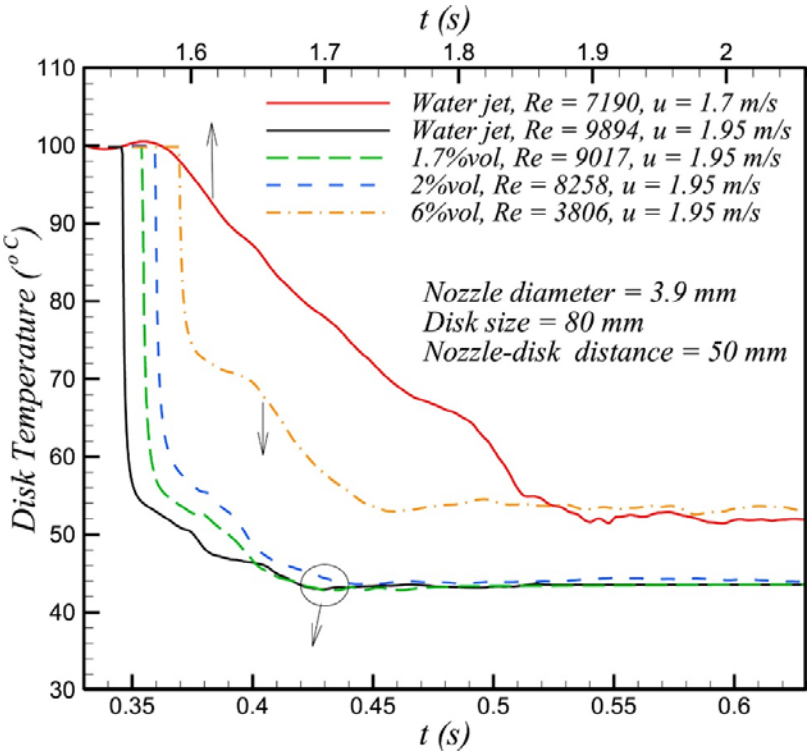

Fig. 6. Evolution of disk average temperature by time for different nanoparticles volume fractions.

It is noted that the trend for disk temperature found in Fig. 6 is highly similar to the experimental measurements conducted by Modak et al. [47]. It is found that the cooling time is increasing with adding to nanoparticles volume fraction. It can be caused by the increase in viscosity and consequently delay in flowing of nanofluid on the surface. This could also be explained through the trend in Prandtl number in Fig. 7. Prandtl number is the proportion of flow to conduction diffusion. For volume fraction below 3%, there is a slight change in Prandtl number, which causes a small difference in cooling duration up to 2% vol. in Fig. 6. The drastic increase in Prandtl number in 6% vol. means the higher impact of viscous force and slower cooling process, also captured in 6% vol. Nonetheless, the trend may change regarding the cooling duration and nanofluid volume fraction if there is boiling on the surface, as the surface is mainly covered with the bubbles and not fluid, reported by Modak et al. [47].

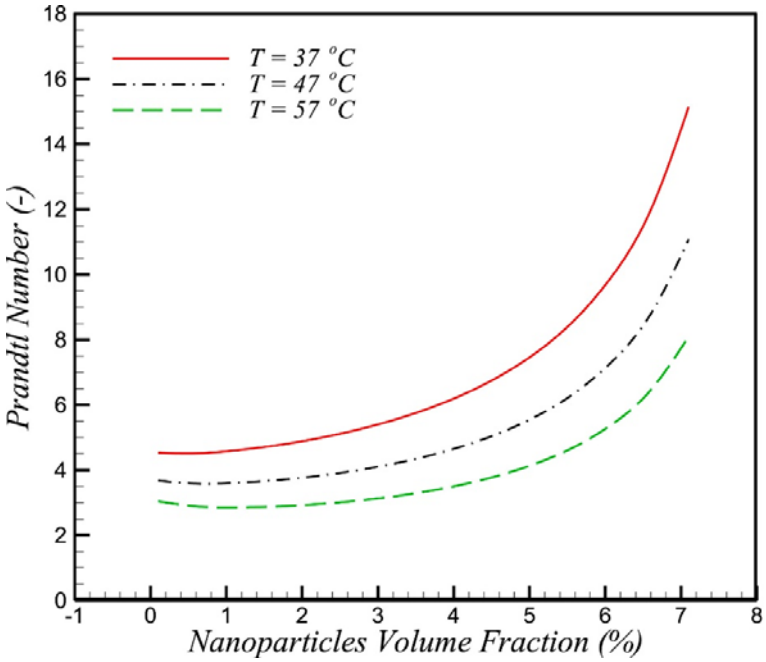

Fig. 7. Dependency of Prandtl number to nanoparticles volume fraction for different temperature.

The effects of rotating disk on heat transfer enhancement are shown in Fig. 8. Non-dimensional rotational Reynolds number is defined to consider the impacts of nanofluid and angular velocity as:

$$\mathrm{Re}_r = \frac{\rho \omega_r D}{\mu} \tag{35}$$

where ω_r is angular velocity in terms of Rad/s.

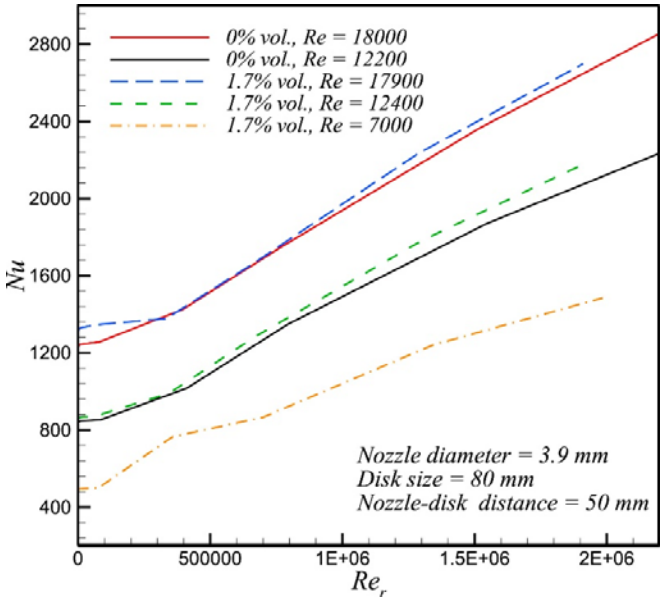

Fig. 8. Nusselt number improvement with rotational Reynolds number at constant jet Re number for different nanoparticles volume fraction.

Heat transfer is not affected by increasing the angular velocity at smaller rotational Re number up to 100, 000, presented in Fig. 8. Nu number shows a linear increase for rotational Re number above 100, 000, no matter of nanoparticles volume fraction. Also, the higher value of Nu number is seen for the case of nanofluid compared to pure water at the same jet inlet Re number. The behaviour of Nu number can be explained by understanding the velocity vectors on the hot disk in Fig. 9. For Re_r below 10^5, the radial velocity is dominant and tangential velocity comes into picture only close to the edge of the disk, as shown in Fig. 9a.

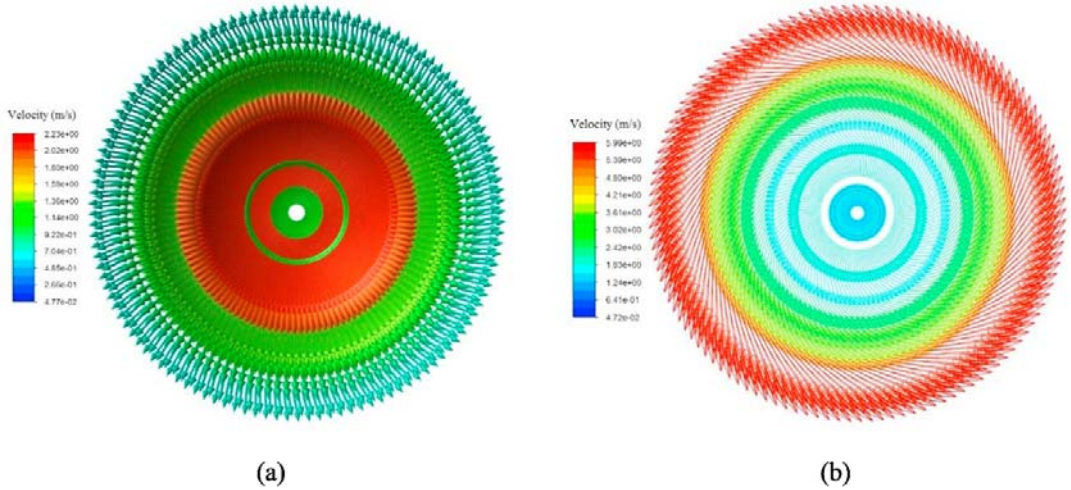

Fig. 9. Velocity vectors for the hot rotating disk from the cntere to the edge at a) Re = 12,500, Re_r = 80,000 b) Re = 12,500, $Re_r = 1.5 \times 10^6$.

It means that heat transfer is still similar to the case without rotation. With strong tangential velocity in $Re_r = 1.5 \times 10^6$, the angular velocity plays an important role in cooling, and contrary to Fig. 9a where the region with higher velocity is close to the centre, the higher velocity magnitude occurs close to the disk edge.

To understand the impact of nanofluid in combination with rotating disk, Fig. 10 is presented. It is expected to observe an increase in heat transfer by adding nanofluid as it goes up to 6% vol. It can be said that adding angular velocity and improving fluid thermal properties by adding nanoparticles should have positive impacts on Nu number. However, the negative side is revealed when the relation between the rotational Re number and obtaining angular velocity is illustrated in Fig. 11. As mentioned above, the higher Nu number obtained by increasing the rotational Re number, which is dependent on angular velocity and fluid viscosity. Adding nanofluid up to 6% vol. leads to higher viscosity, which is in inverse proportion with rotational Re number. To boost up Re_r, angular velocity has to go up. As seen in Fig. 11, to obtain the same rotational number, angular velocity needs to increase dramatically from 3% vol. to 6% vol. This will require much higher torque and power, which is counted as negative effects in the cooling systems with higher nanofluid volume fraction. This could also be explained by defining local friction factor as follows:

$$C_f = \frac{\tau_w}{\rho u^2/2} \tag{36}$$

and shown in Fig. 12. As can be seen, friction coefficient remains the same in the stagnation region, no matter the amount of rotational features. Beyond the stagnation region the angular

velocity becomes dominant, and the rate of reduction in friction coefficient considerably decreases for higher rotational Re number.

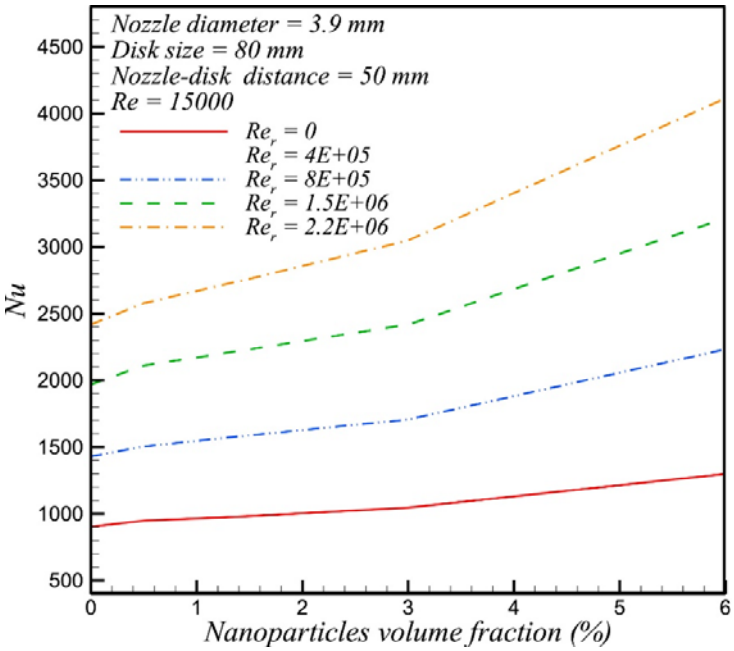

Fig. 10. Nussselt number behaviour with increase in nanoparticles volume fraction for various rotational Reynolds numbers.

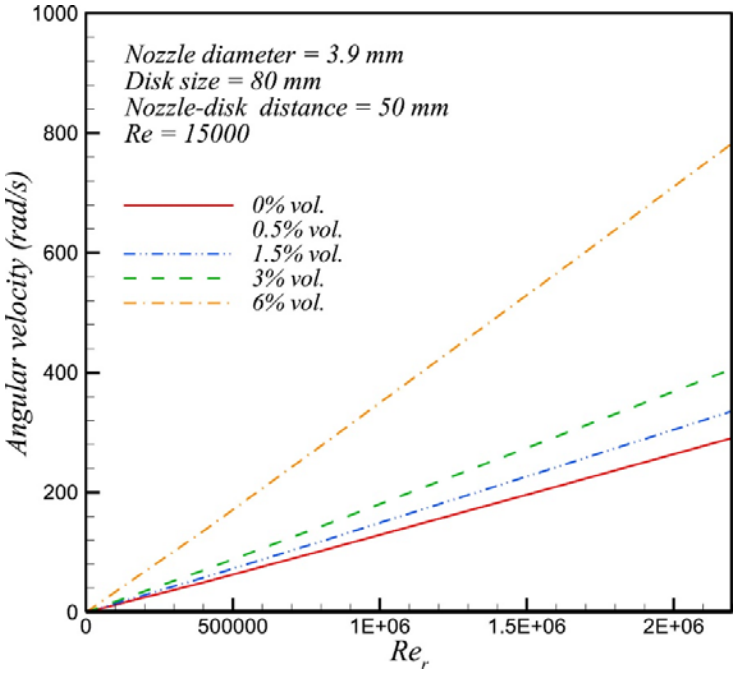

Fig. 11. Correlation between disk angular velocity and rotational Re number for different nanoparticles volume fraction.

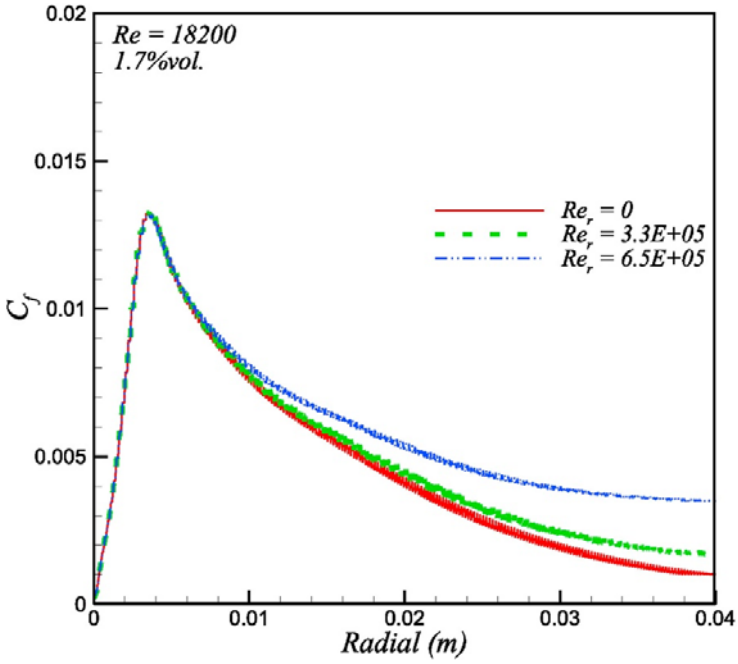

Fig. 12. Local friction coefficient in radial direction on the rotating disk according to rotational Reynolds number.

Regarding average Nu number behavior mentioned here, it is important to locally analyse heat transfer and fluid flow. Local heat transfer coefficient in radial direction from the centre of the disk for two rotational Re number is shown in Fig. 13 for the case of water. The trend is considerably different and needs to be explained, and both pure water and nanofluid showed the same trend. For lower rotational Re number, the trend is expected to be similar to flow on a flat plate heat transfer after stagnation area, starting from higher value and decreasing towards the edge of the disk. On the other hand, heat transfer for higher angular velocity is affected by tangential velocity after point C. The points indicated in Fig. 13 can be detailed as follows:

(1) Point A: Stagnation point at the centre of the disk.
(2) A to B: Stagnation region as also illustrated in Fig. 14.
(3) B to C: Flow in touch with the wall begins at point B, and the boundary layer starts growing, also shown in Fig. 14.
(4) C to D: As radial distance goes further, tangential velocity ($r \times \omega$) contributes to radial velocity and improves heat transfer coefficient.
(5) D to E: The contribution of both tangential and radial velocity gradually decreases because of fluid viscosity, similar to heat transfer on a flat plate.

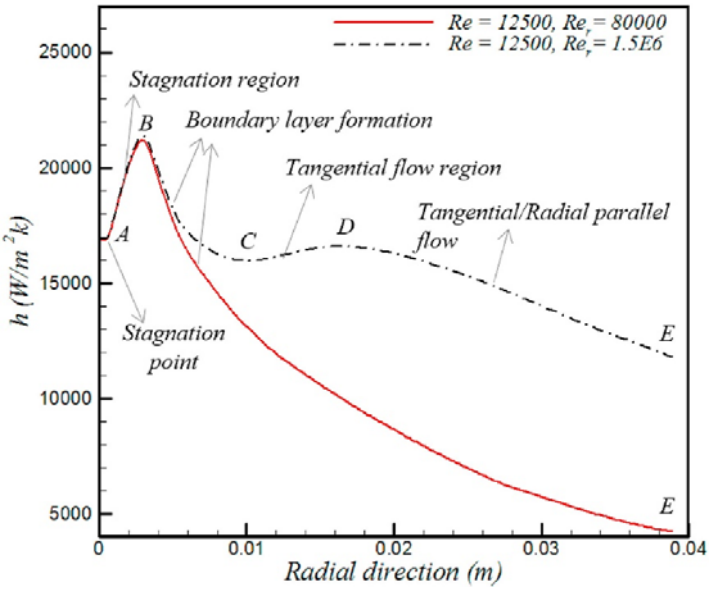

Fig. 13. Classification of water flowing jet on a disk based on radial heat transfer coefficient.

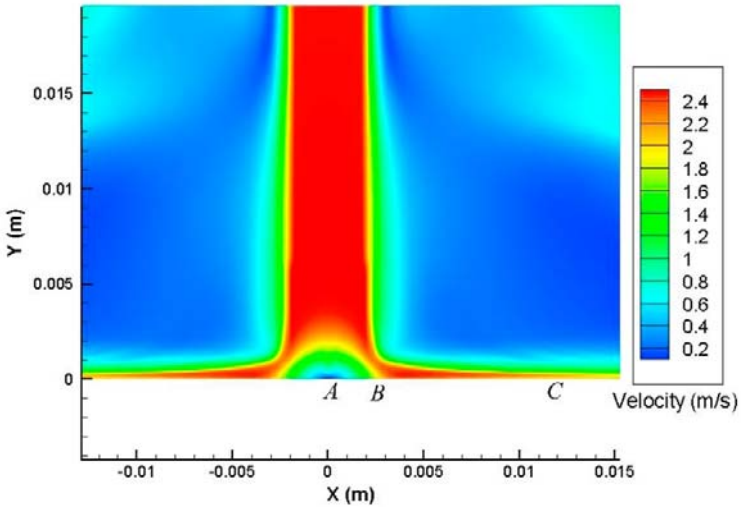

Fig. 14. Velocity contour of jet impingement on the side view and stages of flowing.

Due to the high dependency of Nu to the velocity field, the trend in velocity should also show the growth of the viscous boundary layer, as presented in Fig. 15. Particles are tracked in Lagrangian frame from inlet until they left the domain. A sudden drop in nanoparticles velocity occurs in stagnation region from A to B. The sharp points in velocity profiles are caused by sudden changes of velocity from nozzle inlet to nearly zero at the stagnation point, and immediately after that flowing on the surface by gaining the momentum again. Boundary layer growth between B and C, and eventually tangential velocity due to disk angular velocity increases the particles velocity magnitude from C to D. The nanoparticles velocity evolution from nozzle inlet is in agreement with local heat transfer coefficient and boundary layer growth in Fig. 13. It is noted that the time frame in Fig. 15 is Lagrangian which is completely different than the transient time scale used in the simulation. This Lagrangian time frame is used to track the nanoparticles in the flow moving from one computational cell to another as a parcel regarding the flow velocity.

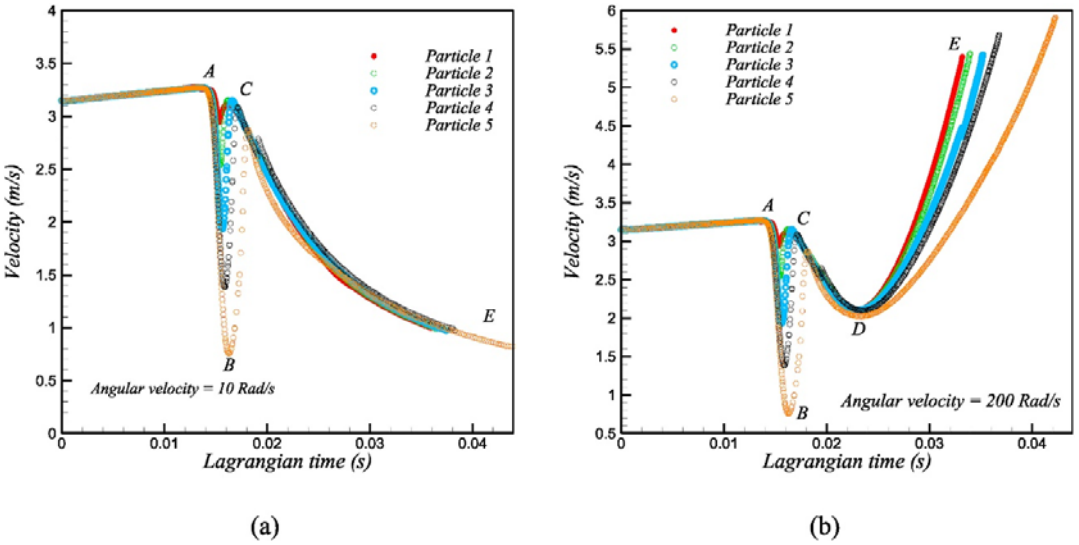

Fig. 15. Evolution of particle velocity magnitude from nozzle inlet to outlet of domain using discrete phase model in Lagrangian time frame.

5. Conclusion

Nanofluid free impingement jet for cooling a stationary and rotating disk with uniform heat flux is numerically investigated. The VOF from multiphase model is used to solve the interaction between air and liquid interface, combined with the discrete phase model to track the nanoparticles in the fluid flow. It is found that the liquid layer is very thin on the disk, and it is crucial to have a few number of mesh inside the boundary layer. The initial simulations are compared with Nu number obtained from experimental literature studies and found in good agreement. Numerical modelling shows that there are six stages in the jet impingement process on a disk until it reaches the steady-state condition. The main difference between stationary and rotating disk is the splatter of droplets and returned to the main flow in stage (4), which is absent in rotating disk. Both adding nanofluid and rotating disk has positive impacts on heat transfer; however, the power cost of rotating in connection with nanofluid increases due to the higher value of viscosity compared to pure water. During analysing local heat transfer coefficient on the hot disk, five fluid regions are identified for rotating disk with rotational Re number above 100, 000. While these regions are reduced to three for the case of the stationary disk and lower rotational Re number. This is caused by dominating the tangential velocity induced by disk angular velocity, as flow moves away from the centre of the disk. The existence of these regions is correctly confirmed by tracking the nanoparticles and checking the evolution of velocity magnitude from jet inlet to outlet of the domain.

One of the major challenges for the jet cooling system is how to model evaporation and boiling on the surface. This can be a part of future studies, as well as considering the impact of nanoparticles.

Declaration of competing interest

The authors declare that they have no known competing financial interests or personal relationships that could have appeared to influence the work reported in this paper.

Acknowledgements

This work was supported by the National Natural Science Foundation of China (Grant No. 51779262). The authors wish to thank the reviewers for their careful, unbiased, and constructive suggestions, which led to this revised manuscript.

References

[1] M. Kahani, M.H. Ahmadi, A. Tatar, M. Sadeghzadeh, Development of multilayer perceptron artificial neural network (MLP-ANN) and least square support vector machine (LSSVM) models to predict Nusselt number and pressure drop of TiO 2/water nanofluid flows through non-straight pathways, Numer. Heat Tran. 74 (2018) 1190–1206, https://doi.org/10.1080/10407782.2018.1523597.
[2] M.H. Ahmadi, A. Baghban, M. Sadeghzadeh, M. Hadipoor, M. Ghazvini, Evolving connectionist approaches to compute thermal conductivity of TiO2/water nanofluid, Phys. A Stat. Mech. Its Appl. (2019) 122489, https://doi.org/10.1016/J.PHYSA.2019.122489.
[3] M.H. Ahmadi, M. Ghazvini, M. Sadeghzadeh, M. Alhuyi Nazari, M. Ghalandari, Utilization of hybrid nanofluids in solar energy applications: a review, Nano-Struct. Nano-Object. 20 (2019) 100386, https://doi.org/10.1016/J.NANOSO.2019.100386.
[4] M.H. Ahmadi, M. Sadeghzadeh, H. Maddah, A. Solouk, R. Kumar, K. Chau, Precise smart model for estimating dynamic viscosity of SiO2/ethylene glycol–water nanofluid, Eng. Appl. Comput. Fluid Mech. 13 (2019) 1095–1105, https://doi.org/10.1080/19942060.2019.1668303.
[5] F. Nasirzadehroshenin, M. Sadeghzadeh, A. Khadang, H. Maddah, M.H. Ahmadi, H. Sakhaeinia, L.G. Chen, Modeling of heat transfer performance of carbon nanotube nanofluid in a tube with fixed wall temperature by using ANN-GA, Eur. Phys. J. Plus. 135 (2020) 217, https://doi.org/10.1140/epjp/s13360-020-00208-y.

[6] M. Ramezanizadeh, M.A. Ahmadi, M.H. Ahmadi, M. Alhuyi Nazari, Rigorous smart model for predicting dynamic viscosity of Al2O3/water nanofluid, J. Therm. Anal. Calorim. 1 (2018), https://doi.org/10.1007/s10973-018-7916-1.
[7] M. Ramezanizadeh, M.H. Ahmadi, M. Alhuyi Nazari, M. Sadeghzadeh, L.G. Chen, A review on the utilized machine learning approaches for modeling the dynamic viscosity of nanofluids, Renew. Sustain. Energy Rev. 114 (2019) 109345, https://doi.org/10.1016/J.RSER.2019.109345.
[8] H.J. Carper, J.J. Saavedra, T. Suwanprateep, Liquid jet impingement cooling of a rotating disk, J. Heat Tran. 108 (1986) 540–546, https://doi.org/10.1115/1.3246968.
[9] R.J. Goldstein, A.I. Behbahani, K.K. Heppelmann, Streamwise distribution of the recovery factor and the local heat transfer coefficient to an impinging circular air jet, Int. J. Heat Mass Tran. 29 (1986) 1227–1235, https://doi.org/10.1016/0017-9310(86)90155-9.
[10] S. Brodersen, D. Metzger, Experimental investigation of the flowfield resulting from the interaction between an impinging jet and a rotating disk, Exp. Therm. Fluid Sci. 5 (1992) 351–358, https://doi.org/10.1016/0894-1777(92)90080-O.
[11] L.A. Gabour, J.H. Lienhard, Wall roughness effects on stagnation-point heat transfer beneath an impinging liquid jet, J. Heat Tran. 116 (1994) 81–87, https://doi.org/10.1115/1.2910887.
[12] Y. Minagawa, S. Obi, Development of turbulent impinging jet on a rotating disk, Int. J. Heat Fluid Flow 25 (2004) 759–766, https://doi.org/10.1016/j.ijheatfluidflow.2004.05.013.

[13] J.B. Baonga, H. Louahlia-Gualous, M. Imbert, Experimental study of the hydrodynamic and heat transfer of free liquid jet impinging a flat circular heated disk, Appl. Therm. Eng. 26 (2006) 1125–1138, https://doi.org/10.1016/j.applthermaleng.2005.11.001.
[14] J.B.T. Moulson, S.I. Green, Effect of ambient air on liquid jet impingement on a moving substrate, Phys. Fluids 25 (2013), https://doi.org/10.1063/1.4823726,0–11.
[15] Z. Jing-Zhou, T. Xiao-Ming, Z. Xing-Dan, Investigation on convective heat transfer over a rotating disk with bottom wall subjected to uniform heat flux, Appl. Mech. Mater. 249–250 (2013) 443–451. https://dx.doi.org/10.4028/www.scientific.net /AMM.249-250.443.
[16] T.H. New, J. Long, Dynamics of laminar circular jet impingement upon convex cylinders, Phys. Fluids 27 (2015), https://doi.org/10.1063/1.4913498.
[17] R. Wu, Y. Fan, T. Hong, H. Zou, R. Hu, X. Luo, An immersed jet array impingement cooling device with distributed returns for direct body liquid cooling of high power electronics, Appl. Therm. Eng. 162 (2019) 114259, https://doi.org/10.1016/j.applthermaleng.2019.114259.
[18] M. Zhang, N. Wang, J.C. Han, Overall effectiveness of film-cooled leading edge model with normal and tangential impinging jets, Int. J. Heat Mass Tran. 139 (2019) 193–204, https://doi.org/10.1016/j.ijheatmasstransfer.2019.05.037.
[19] T.W. Wei, H. Oprins, V. Cherman, G. Van der Plas, I. De Wolf, E. Beyne, M. Baelmans, Experimental characterization and model validation of liquid jet impingement cooling using a high spatial resolution and programmable thermal test chip, Appl. Therm. Eng. 152 (2019) 308–318, https://doi.org/10.1016/j.applthermaleng.2019.02.075.
[20] S. Pachpute, B. Premachandran, Turbulent multi-jet impingement cooling of a heated circular cylinder, Int. J. Therm. Sci. 148 (2020) 106167, https://doi.org/10.1016/j.ijthermalsci.2019.106167.
[21] S. Harmand, J. Pellé, S. Poncet, I.V. Shevchuk, Review of fluid flow and convective heat transfer within rotating disk cavities with impinging jet, Int. J. Therm. Sci. 67 (2013) 1–30, https://doi.org/10.1016/j.ijthermalsci.2012.11.009.
[22] M. Turkyilmazoglu, Effects of uniform radial electric field on the MHD heat and fluid flow due to a rotating disk, Int. J. Eng. Sci. 51 (2012) 233–240, https://doi.org/10.1016/j.ijengsci.2011.09.011.
[23] M. Turkyilmazoglu, Free and circular jets cooled by single phase nanofluids, Eur. J. Mech. B Fluid 76 (2019) 1–6, https://doi.org/10.1016/j.euromechflu.2019.01.009.
[24] M. Turkyilmazoglu, Unsteady mhd flow with variable viscosity: applications of spectral scheme, Int. J. Therm. Sci. 49 (2010) 563–570, https://doi.org/10.1016/j.ijthermalsci.2009.10.007.
[25] F. Selimefendigil, H.F. €Oztop, Effects of nanoparticle shape on slot-jet impingement cooling of a corrugated surface with nanofluids, J. Therm. Sci. Eng. Appl. 9 (2017) 1–8, https://doi.org/10.1115/1.4035811.
[26] A.I. Alsabery, F. Selimefendigil, I. Hashim, A.J. Chamkha, M. Ghalambaz, Fluid-structure interaction analysis of entropy generation and mixed convection inside a cavity with flexible right wall and heated rotating cylinder, Int. J. Heat Mass Tran. 140 (2019) 331–345.
[27] F. Selimefendigil, H.F. €Oztop, Jet impingement cooling and optimization study for a partly curved isothermal surface with CuO-water nanofluid, Int. Commun. Heat Mass Tran. 89 (2017) 211–218, https://doi.org/10.1016/j.icheatmasstransfer.2017.10.007.
[28] H.F. Oztop, Y. Varol, A. Koca, M. Firat, B. Turan, I. Metin, Experimental investigation of cooling of heated circular disc using inclined circular jet, Int. Commun. Heat Mass Tran. 38 (2011) 990–1001, https://doi.org/10.1016/j.icheatmasstransfer.2011.04.013.
[29] F. Selimefendigil, H.F. €Oztop, Pulsating nanofluids jet impingement cooling of a heated horizontal surface, Int. J. Heat Mass Tran. 69 (2014) 54–65, https://doi.org/10.1016/j.ijheatmasstransfer.2013.10.010.

[30] F. Selimefendigil, H.F. €Oztop, Analysis and predictive modeling of nanofluid-jet impingement cooling of an isothermal surface under the influence of a rotating cylinder, Int. J. Heat Mass Tran. 121 (2018) 233–245, https://doi.org/10.1016/j.ijheatmasstransfer.2018.01.008.
[31] M. Ramezanizadeh, M. Alhuyi Nazari, M. Hossein Ahmadi, L.G. Chen, A review on the approaches applied for cooling fuel cells, Int. J. Heat Mass Tran. 139 (2019) 517–525, https://doi.org/10.1016/J.IJHEATMASSTRANSFER.2019.05.032.
[32] M.H. Ahmadi, M. Ghazvini, A. Baghban, M. Hadipoor, P. Seifaddini, Computing approaches for thermal C onductivity estimation of CNT/water nanofluid, Rev. Des Compos. Des Matériaux Avancés Soft. 29 (2019) 71–82.
[33] M.H. Ahmadi, A. Tatar, P. Seifaddini, M. Ghazvini, R. Ghasempour, M.A. Sheremet, Thermal conductivity and dynamic viscosity modeling of Fe 2 O 3/water nanofluid by applying various connectionist approaches, Numer. Heat Tran. 74 (2018) 1301–1322, https://doi.org/10.1080/10407782.2018.1505092.
[34] Y. He, Y. Jin, H. Chen, Y. Ding, D. Cang, H. Lu, Heat transfer and flow behaviour of aqueous suspensions of TiO 2 nanoparticles (nanofluids) flowing upward through a vertical pipe, Int. J. Heat Mass Tran. 50 (2007) 2272–2281.
[35] H. Ghodsinezhad, M. Sharifpur, J.P.J.P. Meyer, Experimental investigation on cavity flow natural convection of Al2O3–water nanofluids, Int. Commun. Heat Mass Tran. 76 (2016) 316–324, https://doi.org/10.1016/j.icheatmasstransfer.2016.06.005.
[36] W.H. Azmi, N.A. Usri, R. Mamat, K.V. Sharma, M.M. Noor, Force convection heat transfer of Al2O3 nanofluids for different based ratio of water: ethylene glycol mixture, Appl. Therm. Eng. 112 (2017) 707–719, https://doi.org/10.1016/j.applthermaleng.2016.10.135.
[37] M. Sharifpur, N. Tshimanga, J.P. Meyer, O. Manca, Experimental investigation and model development for thermal conductivity of α-Al2O3-glycerol nanofluids, Int. Commun. Heat Mass Tran. 85 (2017) 12–22, https://doi.org/10.1016/j.icheatmasstransfer.2017.04.001.
[38] N. Tshimanga, M. Sharifpur, J.P. Meyer, Experimental investigation and model development for thermal conductivity of glycerol–MgO nanofluids, Heat Tran. Eng. 37 (2016) 1538–1553, https://doi.org/10.1080/01457632.2016.1151297.
[39] O. Zeitoun, M. Ali, Nanofluid impingement jet heat transfer, Nanoscale Res. Lett. 7 (2012) 139, https://doi.org/10.1186/1556-276X-7-139.
[40] C.T. Nguyen, N. Galanis, G. Polidori, S. Fohanno, C.V. Popa, A. Le Bechec, An experimental study of a confined and submerged impinging jet heat transfer using Al2O3-water nanofluid, Int. J. Therm. Sci. 48 (2009) 401–411, https://doi.org/10.1016/j.ijthermalsci.2008.10.007.
[41] S.D. Barewar, S. Tawri, S.S. Chougule, Heat transfer characteristics of free nanofluid impinging jet on flat surface with different jet to plate distance: an experimental investigation, Chem. Eng. Process. - Process Intensif. 136 (2019) 1–10, https://doi.org/10.1016/j.cep.2018.12.001.
[42] K. Wongcharee, V. Chuwattanakul, S. Eiamsa-ard, Influence of CuO/water nanofluid concentration and swirling flow on jet impingement cooling, Int. Commun. Heat Mass Tran. 88 (2017) 277–283, https://doi.org/10.1016/j.icheatmasstransfer.2017.08.020.
[43] K. Wongcharee, V. Chuwattanakul, S. Eiamsa-ard, Chemical Engineering and Processing : Process Intensi Fi Cation Heat Transfer of Swirling Impinging Jets with TiO 2 -water Nano Fl Uids, vol. 114, 2017, pp. 16–23, https://doi.org/10.1016/j.cep.2017.01.004.
[44] A. AbdElHady, Experimental Investigation of Pool Boiling and Boiling under Submerged Impinging Jet of Nanofluids, McMaster University, 2013.

[45] J. Lv, C. Hu, M. Bai, K. Zeng, S. Chang, D. Gao, Experimental investigation of free single jet impingement using SiO2-water nanofluid, Exp. Therm. Fluid Sci. 84 (2017) 39–46, https://doi.org/10.1016/j.expthermflusci.2017.01.010.
[46] M.M. Sorour, W.M. El-Maghlany, M.A. Alnakeeb, A.M. Abbass, Experimental study of free single jet impingement utilizing high concentration SiO2 nanoparticles water base nanofluid, Appl. Therm. Eng. 160 (2019) 114019, https://doi.org/10.1016/j.applthermaleng.2019.114019.
[47] M. Modak, S.S. Chougule, S.K. Sahu, An experimental investigation on heat transfer characteristics of hot surface by using CuO-water nanofluids in circular jet impingement cooling, J. Heat Tran. 140 (2018) 1–10, https://doi.org/10.1115/1.4037396.
[48] B. Sun, Y. Qu, D. Yang, Heat transfer of single impinging jet with Cu nanofluids, Appl. Therm. Eng. 102 (2016) 701–707, https://doi.org/10.1016/j.applthermaleng.2016.03.166.
[49] J.C. Lallave, M.M. Rahman, A. Kumar, Numerical analysis of heat transfer on a rotating disk surface under confined liquid jet impingement, Int. J. Heat Fluid Flow 28 (2007) 720–734, https://doi.org/10.1016/j.ijheatfluidflow.2006.09.005.
[50] H. Lamraoui, K. Mansouri, R. Saci, Numerical investigation on fluid dynamic and thermal behavior of a non-Newtonian Al 2 O 3 –water nanofluid flow in a confined impinging slot jet, J. Nonnewton. Fluid Mech. 265 (2019) 11–27, https://doi.org/10.1016/j.jnnfm.2018.12.011.
[51] A.A. Avramenko, I.V. Shevchuk, S. Abdallah, D.G. Blinov, A.I. Tyrinov, Self-similar analysis of fluid flow, heat, and mass transfer at orthogonal nanofluid impingement onto a flat surface, Phys. Fluids 29 (2017), https://doi.org/10.1063/1.4983061.
[52] Y.T. Yang, Y.H. Wang, J.C. Hsu, Numerical thermal analysis and optimization of a water jet impingement cooling with VOF two-phase approach, Int. Commun. Heat Mass Tran. 68 (2015) 162–171, https://doi.org/10.1016/j.icheatmasstransfer.2015.08.010.
[53] M.M. Rehman, Z.G. Qu, R.P. Fu, H.T. Xu, Numerical study on free-surface jet impingement cooling with nanoencapsulated phase-change material slurry and nanofluid, Int. J. Heat Mass Tran. 109 (2017) 312–325, https://doi.org/10.1016/j.ijheatmasstransfer.2017.01.094.
[54] R. Oguic, S. Poncet, S. Viazzo, High-order direct numerical simulations of a turbulent round impinging jet onto a rotating heated disk in a highly confined cavity, Int. J. Heat Fluid Flow 61 (2016) 366–378, https://doi.org/10.1016/j.ijheatfluidflow.2016.05.013.
[55] R. Manceau, R. Perrin, M. Hadžiabdić, S. Benhamadouche, Investigation of the interaction of a turbulent impinging jet and a heated, rotating disk, Phys. Fluids 26 (2014), https://doi.org/10.1063/1.4867380.
[56] W. Peng, L. Jizu, B. Minli, W. Yuyan, H. Chengzhi, A numerical investigation of impinging jet cooling with nanofluids, Nanoscale Microscale Thermophys. Eng. 18 (2014) 329–353, https://doi.org/10.1080/15567265.2014.921749.
[57] M. Mahdavi, M. Sharifpur, H. Ghodsinezhad, J.P. Meyer, A new combination of nanoparticles mass diffusion flux and slip mechanism approaches with electrostatic forces in a natural convective cavity flow, Int. J. Heat Mass Tran. 106 (2017) 980–988, https://doi.org/10.1016/j.ijheatmasstransfer.2016.10.065.
[58] M. Mahdavi, M. Sharifpur, J.P. Meyer, Implementation of diffusion and electrostatic forces to produce a new slip velocity in the multiphase approach to nano fluids, Powder Technol. 307 (2017) 153–162.
[59] M. Mahdavi, M. Sharifpur, J.P. Meyer, Discrete modelling of nanoparticles in mixed convection flows, Powder Technol. 338 (2018) 243–252, https://doi.org/10.1016/j.powtec.2018.07.025.

[60] C.W. Hirt, B. Nicholas, Volume of fluid (VOF) method for the dynamics of free boundaries, J. Comput. Phys. 39 (1981) 201–225, https://doi.org/10.1016/0021-9991(81)90145-5.
[61] J.U. Brackbill, D.B. Kothe, C. Zemach, A continuum method for modeling surface tension, J. Comput. Phys. 100 (1992) 335–354, https://doi.org/10.1016/0021-9991(92)90240-Y.
[62] E. Bacharoudis, M.G. Vrachopoulos, M.K. Koukou, D. Margaris, A.E. Filios, S. A. Mavrommatis, Study of the natural convection phenomena inside a wall solar chimney with one wall adiabatic and one wall under a heat flux, Appl. Therm. Eng. 27 (2007) 2266–2275, https://doi.org/10.1016/j.applthermaleng.2007.01.021.
[63] C. Teodosiu, F. Kuznik, R. Teodosiu, CFD modeling of buoyancy driven cavities with internal heat source - application to heated rooms, Energy Build. 68 (2014) 403–411, https://doi.org/10.1016/j.enbuild.2013.09.041.
[64] M. Mahdavi, M. Sharifpur, H. Ghodsinezhad, J.P. Meyer, Experimental and numerical investigation on a water-filled cavity natural convection to find the proper thermal boundary conditions for simulations, Heat Tran. Eng. 39 (2018) 359–373, https://doi.org/10.1080/01457632.2017.1305835.
[65] M. Sharifpur, S. Yousefi, J.P. Meyer, A new model for density of nanofluids including nanolayer, Int. Commun. Heat Mass Tran. 78 (2016) 168–174, https://doi.org/10.1016/j.icheatmasstransfer.2016.09.010.
[66] M. Corcione, Empirical correlating equations for predicting the effective thermal conductivity and dynamic viscosity of nanofluids, Energy Convers. Manag. 52 (2011) 789–793, https://doi.org/10.1016/j.enconman.2010.06.072.
[67] H.P. Meissner, A.S. Michaels, Surface tensions of pure liquids and liquid mixtures, Ind. Eng. Chem. 41 (1949) 2782–2787.
[68] Y. Wang, J. Wu, Numerical simulation on single bubble behavior during Al2O3/H2O nanofluids flow boiling using Moving Particle Simi-implicit method, Prog. Nucl. Energy 85 (2015) 130–139, https://doi.org/10.1016/j.pnucene.2015.06.017.
[69] M. Mahdavi, M. Sharifpur, J.P. Meyer, Natural convection study of Brownian nano-size particles inside a water-filled cavity by Lagrangian-Eulerian tracking approach, in: Heat Transf., International Conference on Heat Transfer, Fluid Mechanics and Thermodynamics (HEFAT2016), Costa del Sol, Malaga, Spain, 2016, p. 17.
[70] A. Li, G. Ahmadi, Dispersion and deposition of spherical particles from point sources in a turbulent channel flow, Aerosol Sci. Technol. 16 (1992) 209–226, https://doi.org/10.1080/02786829208959550.
[71] X. Zheng, Z. Silber-li, The influence of Saffman lift force on nanoparticle concentration distribution near a wall, Appl. Phys. Lett. 95 (2009) 124105, https://doi.org/10.1063/1.3237159.
[72] B. Oesterle, T.B. Dinh, Experiments on the lift of a spinning sphere in a range of intermediate Reynolds numbers, Exp. Fluid 25 (1998) 16–22, https://doi.org/10.1007/s003480050203.
[73] G.S. McNab, A. Meisen, Thermophoresis in liquids, J. Colloid Interface Sci. 44 (1973) 339–346, https://doi.org/10.1016/0021-9797(73)90225-7.
[74] Y. Guo, S. Green, Visualization of high speed liquid jet impaction on a moving surface, J. Vis. Exp. 98 (2015) 1–12, https://doi.org/10.3791/52603.